Crystallization Mechanisms of Hemoglobin C in the R State

Angela R. Feeling-Taylor,* S.-T. Yau,‡ Dimiter N. Petsev,† Ronald L. Nagel,§¶ Rhoda Elison Hirsch,*¶ and Peter G. Vekilov†

*Department of Anatomy and Structural Biology, Albert Einstein College of Medicine and Montefiore Hospital, Comprehensive Sickle Cell Center, The Bronx, New York; †Department of Chemical Engineering, University of Houston, Houston, Texas; ‡Department of Physics, Hunter College of the City University of New York, New York; and ¶Department of Medicine (Division of Hematology) and §Department of Physiology and Biophysics, Albert Einstein College of Medicine and Montefiore Hospital, Comprehensive Sickle Cell Center, The Bronx, New York

ABSTRACT Crystallization of the mutated hemoglobin, HbC, which occurs inside red blood cells of patients expressing β^C-globin and exhibiting the homozygous CC and the heterozygous SC (in which two mutant β-globins, S and C, are expressed) diseases, is a convenient model for processes underlying numerous condensation diseases. As a first step, we investigated the molecular-level mechanisms of crystallization of this protein from high-concentration phosphate buffer in its stable carbomonoxy form using high-resolution atomic force microscopy. We found that in conditions of equilibrium with the solution, the crystals' surface reconstructs into four-molecule-wide strands along the crystallographic *a* (or *b*) axis. However, the crystals do not grow by the alignment of such preformed strands. We found that the crystals grow by the attachment of single molecules to suitable sites on the surface. These sites are located along the edges of new layers generated by two-dimensional nucleation or by screw dislocations. During growth, the steps propagate with random velocities, with the mean being an increasing function of the crystallization driving force. These results show that the crystallization mechanisms of HbC are similar to those found for other proteins. Therefore, strategies developed to control protein crystallization in vitro may be applicable to pathology-related crystallization systems.

INTRODUCTION

Hemoglobin (Hb) C is a mutated Hb, which differs from the most common variant, HbA, by a single mutation at the sixth amino acid position of the β subunit that replaces the negatively charged glutamic acid with a positively charged lysine (β^6 Glu→Lys) (Hunt and Ingram, 1958). In its oxygenated, R state, HbC forms crystals inside red blood cells. The intraerythrocytic crystals contribute to the clinical pathogenesis of the CC disease, a mild and chronic hemolytic anemia (Lawrence et al., 1991; Lessin et al., 1969). Oxy-HbC crystals also form in red cells of patients with the SC disease, who are doubly heterozygous for both HbS and HbC. SC disease is a severe, life-threatening condition (Nagel and Lawrence, 1991). Thus, data on the mechanisms and dynamics of HbC crystallization, including at the molecular level, contributes to the understanding of the pathogenesis of the CC and SC diseases, and may be relevant to the other protein condensation diseases: sickle cell anemia (Eaton and Hofrichter, 1990), the eye cataract (Benedek et al., 1999), Alzheimer's (Kelly, 2000), the prion diseases (Bucciantini et al., 2002; Koo et al., 1999), and others.

Previous observations of the formation of HbC crystals in osmotically dehydrated red blood cells were interpreted in terms of a pathway involving formation of small ribbon-like ''paracrystals,'' followed by their alignment into tetragonal and hexagonal crystals (Charache et al., 1967). The suggested mechanism of alignment of the microribbons is similar to the one implied for the other β^6 Hb variant, deoxy-HbS (Bluemke et al., 1988; Lessin et al., 1969; Makinen and Sigountos, 1984; Potel et al., 1984). This pathway is at odds with the crystallization mechanism established for a broad variety of proteins under a broad range of conditions (McPherson et al., 2000; Vekilov and Chernov, 2002)—in all cases crystallization occurs by the association of single molecules into an existing crystal. Thus, in situ monitoring of the elementary acts of molecular attachment to the crystals are needed to decide if indeed hemoglobin crystallization follows a pathway distinct from the one of most other proteins.

In preceding studies, we found that, similar to many other proteins, the solubility of the protein has a strong retrograde dependence on temperature (Feeling-Taylor et al., 1999). We analyzed the thermodynamics of HbC crystallization and found a high positive enthalpy (Vekilov et al., 2002). This means that the specific interactions favor HbC molecules in the solute state, and HbC crystallization is only possible because of a huge entropy gain, likely stemming from the release of up to 10 water molecules per protein intermolecular contact. Such contacts have been defined as hydrophobic attraction (Chandler, 2002; Eisenberg and Kauzmann, 1969). Thus, our data suggest that the greater propensity for R-state HbC crystallization is attributable to the increased hydrophobicity resulting from conformational changes that accompany the HbC mutation. We also found that the interactions between the HbC, HbA, and HbS molecules in solution are

Submitted January 7, 2004, and accepted for publication June 16, 2004.

Address reprint requests to Peter G. Vekilov, Dept. of Chemical Engineering, University of Houston, Houston, TX 77204-4004. Tel.: 713-743-4315; Fax: 713-743-4323; E-mail: vekilov@uh.edu.

Dimiter N. Petsev's present address is Dept. of Chemical and Nuclear Engineering, University of New Mexico, Albuquerque, NM 87131-1341.

0006-3495/04/10/2621/09 $2.00

doi: 10.1529/biophysj.104.039743

dominated by chemically specific binding between the surfaces of Hb molecules that are adjacent in the respective solid phase, and that the contributions of the electrostatic interactions are insignificant at electrolyte concentrations $\geq$0.05 M (Vekilov et al., 2002). These observations do not reveal any specificity of HbC crystallization that may underlie a crystallization mechanism different from the one established for many other proteins. In addition, microscopic observations and determinations of the nucleation statistics showed that the crystals of HbC nucleate and grow by the attachment of native molecules from the solution (Vekilov et al., 2002).

This article is focused on the mechanisms of growth of the HbC crystals. We employ atomic force microscopy (AFM) in situ, during the growth of the crystals from supersaturated solutions, or in saturated solutions, i.e., when the crystals are in a dynamic equilibrium with the solution. Because of the higher stability of CO-HbC compared with Oxy-HbC, we used the carbomonoxy form as representative of the R-state HbC. The structure of carbomonoxy-HbC was recently determined (Dewan et al., 2002) using crystals grown under conditions analogous to those employed here.

Crystallization was carried out at concentration of the potassium phosphate buffer of 1.9 M, at pH 7.35. These high concentrations of the electrolyte significantly lower the solubility of the hemoglobin and allow high relative supersaturations at low concentrations of the precious protein. Attempts to carry out crystallization studies at low buffer concentrations yielded crystals with phosphate in the range 0.6–1.6 M only if polyethylene glycol is added; at even lower phosphate concentrations no crystallization of CO-HbC occurs. The interactions and thermodynamics in protein-water-polymer systems are completely different from a system that does not contain the polymer and we did not consider results obtained with PEG relevant to the goals of this investigation. Obviously, the phosphate concentration used here is significantly higher than the one in the red blood cells. Our failure to obtain crystals at low phosphate concentrations suggests that in vivo crystallization of R-state HbC is a complex phenomenon that depends on many factors. We view the investigations reported here as a first step in the understanding of these processes.

EXPERIMENTAL PROCEDURES

Preparation of human HbC solutions

The procedures for isolation and purification of HbC and for preparation of the solutions of CO-HbC were identical to those described in Hirsch et al. (2001).

Growth of crystals on glass substrates for AFM observations

Coverslips treated with trimethylchlorosilane were glued to iron disks and used as glass substrates for AFM crystal growth studies. 20 μl aliquots of 20 mg mL^{-1} CO-HbC in 1.9 M KH_2PO_4/K_2HPO_4 at pH 7.35 were dispensed on each disk. To avoid evaporation, the droplets were covered with glass covers, hermetically sealed and kept for a few hours in a controlled temperature chamber at ~22°C. Typically, this led to the formation of 3–20 crystals of sizes ranging from 20 to 200 μm firmly attached to the glass bottom. The crystals always had the tetragonal bipyramid habit, consisting of eight {101} faces, typical of the tetragonal crystals of R-state HbC (see, e.g., Hirsch et al., 1988). Droplets with three to five crystals were selected and the crystals were washed by 1.9M KH_2PO_4/K_2HPO_4, pH 7.35. The iron disks with the glass covers holding the crystals were then magnetically mounted on the AFM scanner. The fluid AFM cell was filled with the crystallizing solution and imaging commenced.

Atomic force microscopy observations

We used a multimode atomic force microscope Nanoscope IIIa (Digital Instruments, Santa Barbara, CA). All images were collected in situ during the growth of the crystals using the less intrusive tapping mode. This mode allows visualization of adsorbed protein and impurity species—tip impact in contact imaging mode often prevents such imaging. We used the standard SiN tips. The tapping drive frequency was in the range of 25–31 kHz, within the range used by other authors (Yip and Ward, 1996), adjusted to the resonance value of the used tip. Other scanning parameters were adjusted such that continuous imaging affected neither the surface structure nor the process dynamics. For verification, we varied the scan sizes and the time elapsed between image collections, and saw that neither the spatial nor the temporal characteristics of the processes changed. For details and tests about the determination of the maximum resolution of 16 Å, and the calibration of the AFM imaging technique with other studied proteins, see Yau et al. (2000a). For calibration of the AFM technique with HbC crystals, we note that the experiments with HbC crystals in supersaturated solutions (see below) revealed that the thickness of a layer on a (101) face is ~55 Å, and the periodicity along the [$\bar{1}$01]-axis is ~200 Å, in agreement with the x-ray crystal structure, according to which the respective values should be 53 and 202 Å (Dewan et al., 2002).

The characteristic shape of the crystals with the pyramid apex in the [001] (or *c*) direction allowed an easy correlation between the crystallographic directions and the AFM image orientation.

Temperature control and solubility

Temperature in the laboratory was stabilized to ~22°C. No additional temperature control of the solution in the AFM fluid cell was employed. Insertion of a thermocouple in the crystallizing solution revealed that its temperature was 27 $\pm$ 0.7°C.

The solubility of CO-HbC in the solution with the used composition at the temperature of the crystallization, ~27°C, was determined by monitoring trains of growth steps (see below) and gradually decreasing the CO-HbC concentration in the solution. We found that at $C = 1.2 \pm 0.3$ mg mL^{-1}, the propagation of the steps stopped, and when the concentration was lowered below this value, step movement was backward and the crystal was dissolving. We assign the width of the solubility range to the high sensitivity of the solubility to the concentration of the phosphate buffer: slight variations in the buffer concentration between preparations result in noticeable solubility variations. This value was chosen as the CO-HbC solubility at the temperature of the experiments. It agrees with the value extrapolated from the solubility in the 10–16°C range by using the crystallization enthalpy of 155 kJ mol^{-1} (Vekilov et al., 2002).

RESULTS

The surface of crystals at equilibrium with the solution

To image the surface of a (101) face of a tetragonal crystal of CO-HbC at equilibrium with the solution, a solution with CO-HbC concentration 1.5 mg mL^{-1}, slightly higher than

the solubility at the temperature of the experiments, was pumped into the AFM cell. In a few hours, we examined the whole facet to verify that growth had stopped and equilibrium had been reached. An image of the surface at equilibrium is shown in Fig. 1 *a*. This and other similar images reveal that the molecules in the top crystal layer are arranged in four-molecule-wide strands. The strands are oriented along a [010] direction. The strands are separated by well-defined groves, highlighted in Fig. 1 *a*. The four molecules in the cross-section of a strand appear to be different and at first sight this seems compatible with the crystallographic symmetry group $P4_12_12$ (Dewan et al., 2002). Indeed, the 4_1 axis oriented along the [001] direction, i.e., at an angle with the observed (101) face and perpendicular to the [010] direction, rotates each of the four molecules by 90° with respect to its neighbors in the quartet, exposing different sides of the HbC molecule.

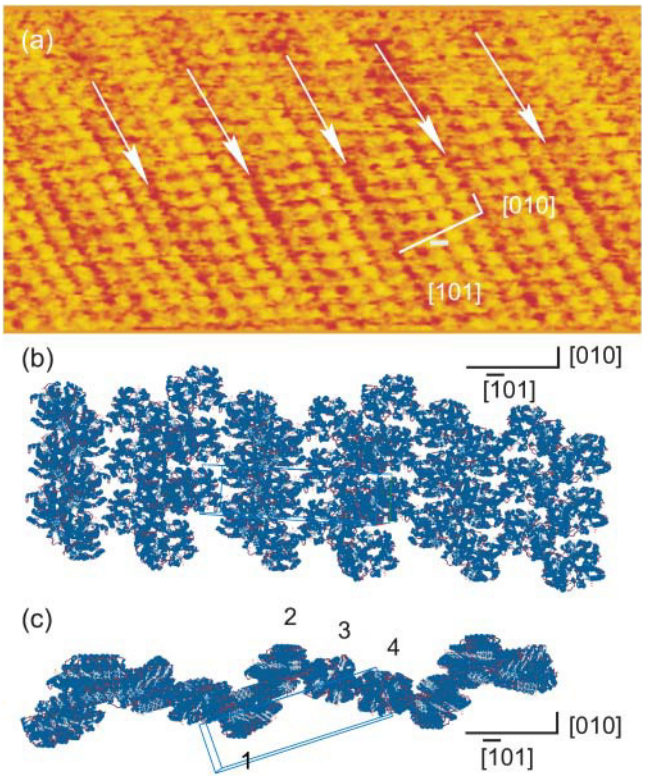

FIGURE 1 The structure of (101) surfaces of CO-HbC crystals at equilibrium with solution. (*a*) Atomic force microscopy characterization of a (101) surface of a CO-HbC crystal in equilibrium with the solution; for details, see text. The (101) cross section of the unit cell is shown. White arrows point at grooves between four-member strands along the *b* axis. (*b* and *c*) Schematic representations of a 3 molecule × 10 molecule section of the (101) surface based on the x-ray crystal structure from Dewan et al. (2002), PDP entry 1k1k. Black right angles only indicate orientation of respective crystallographic directions and the lengths of the shoulders are not related to the respective lattice parameters. Blue parallelograms represent unit cells. Rendered using Swiss PDB Viewer. (*b*) View along the [101] direction, analogous to viewing direction in *a*. (*c*) View along the [010] direction, revealing the variations of the surface height. Arabic numerals mark the four molecules in a unit cell.

For a comparison with the bulk structure of the crystal, Fig. 1, *b* and *c*, shows schematic images of the crystal surface assuming that it reproduces the bulk crystal structure as revealed in Dewan et al. (2002). These figures reveal that if the crystal surface was fully determined by the bulk structure, neither the grooves nor the four member strands should be present, i.e., the surface is reconstructed. The surface reconstruction is discussed in detail below.

The growth mechanisms: generation of new crystal layers

Fig. 2 *a* and many other similar images reveal that the crystals grow by a two step mechanism: 1), new layers are generated by a surface nucleation process; and 2), these layers incorporate building blocks from the solution and spread to cover the whole facet. Note that the generation of a subsequent layer occurs while the underlying layer is still growing. This leads to many layers spreading and chasing and meeting one another on the crystal surface. This crystallization mechanism has been postulated by Volmer in the 1930s (Volmer, 1939) and observed for numerous small-molecule, protein and virus crystals (Giesen et al., 1996; Malkin et al., 1996; McPherson et al., 2000; Yau et al., 2000a; Yip and Ward, 1996).

In a few cases, we saw growth layers initiated by the rotation of a spiral around a screw dislocation outcropping on the monitored surface, Fig. 2 *b*. This mechanism is typical for small-molecule materials (DeYoreo et al., 1994; Gratz et al., 1993; Teng et al., 1998), and has been observed with proteins (Durbin and Carlson, 1992; Durbin and Feher, 1996; Land et al., 1997; Malkin et al., 1996; Reviakine et al., 2003). Note the hollow core around the dislocation axis. The core lowers the strain due to the misfit of the lattice layers at the screw dislocation. Its width is determined by the balance of this strain with the surface free energy between the solution and the crystal. A consistent thermodynamic theory reveals that the core width also depends on the elastic properties of the crystal and the supersaturation (Van den Hoek et al., 1982; Vekilov et al., 1990). Hollow cores around screw dislocation have been seen for many inorganic (De Yoreo et al., 1997) and a protein crystal (Kuznetsov et al., 1999). The significance of the observation of hollow cores with protein crystals is that it indicates that the elastic properties of the protein crystals and their response to lattice strain are not principally different from those of small-molecule crystals (Chernov, 2003; Vekilov and Chernov, 2002).

The growth mechanisms: incorporation of molecules into steps

Zooming in on the edge of the growing layer, Fig. 3, we find that the layer thickness is ~55 Å—close to the prediction of 53 Å based on the x-ray structure (Dewan et al., 2002).

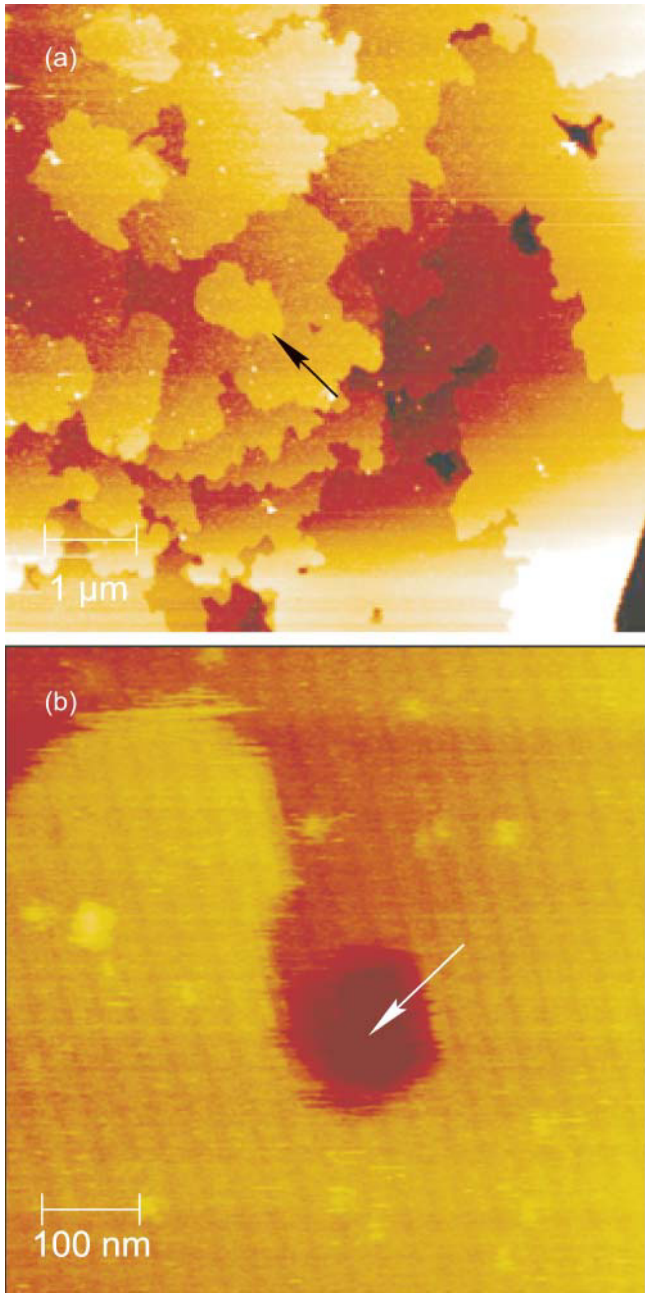

FIGURE 2 Mechanisms of layer generation. (*a*) Layer generation by two-dimensional nucleation, a newly generated layer is indicated by a black arrow, $C_{\text{CO-HbC}} = 3$ mg mL^{-1}. This is a more detailed figure from Vekilov et al. (2003). (*b*) A screw dislocation, with hollow core (*white arrow* points at the center of the hollow core) around it and spiral step that it generates; note that the spiral is left-winged on the crystal surface and right-winged inside the hollow core. $C_{\text{CO-HbC}} = 1$ mg ml^{-1} approximate solubility.

Furthermore, we see that the molecular rows along the *a* (or *b*) axes are in perfect alignment with the underlying layers, as one would expect for the tetragonal lattice of the CO-HbC crystals. The edge of the unfinished layers is rough, and the characteristic lengthscale of the roughness equals one molecular dimension. This is only possible if molecules join the crystal one by one. We conclude that the building blocks of CO-HbC crystals are single protein molecules.

The sequence in Fig. 4 reveals that as the molecules attach to the edges of unfinished top crystal layers, these layers advance and the crystal grows. No correlation exists between the direction of motion of the steps and the crystallographic directions, in agreement with the lower magnification images in Fig. 2, which shows isotropic spreading of the islands and a round dislocation core. Fig. 5 compares the step velocities in the $[\bar{1}\,01]$, [010] , and $[\bar{1}\,\bar{1}\,1]$ crystallographic directions computed from the respective displacements of steps between pairs of images in Fig. 4. We see that the velocities are not steady and randomly change in time because of the intrinsic stochasticity of the molecular incorporation processes, i.e., the number of molecules joining the step for a certain time is a random variable over the times of imaging in Fig. 4. Still, if we average the data for each direction in Fig. 5, we get roughly equal averages, in agreement with the isotropy of step propagation discussed above.

The average velocity from the data in Fig. 6 is $\bar{v} = 1.1$ nm s^{-1}. We can use this value for a rough evaluation of the step kinetic coefficient β, a parameter characterizing the time-averaged kinetics of incorporation of the HbC molecules into crystals. We use the definition of β (Chernov, 1984)

$$\bar{v} = \beta\Omega(C - C_e),$$

where C and C_e are, respectively, the HbC concentration and its solubility in molecules per unit volume, so that $C_e = 1.1$

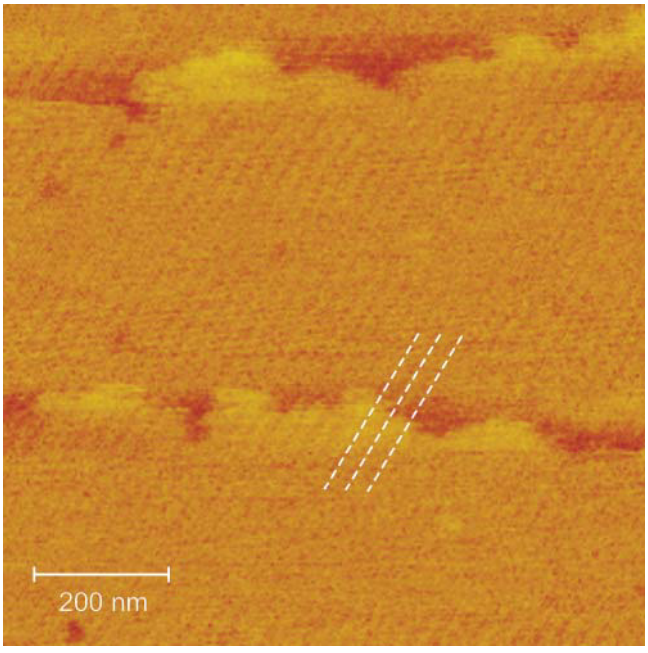

FIGURE 3 Spreading of growth layers with each higher layer in perfect crystallographic alignment with the respective lower layer. White dashed lines highlight continuity between two layers of linear features in a [010] direction. $C_{\text{CO-HbC}} = 2$ mg mL^{-1}. From Fig. 3 in Vekilov et al. (2002).

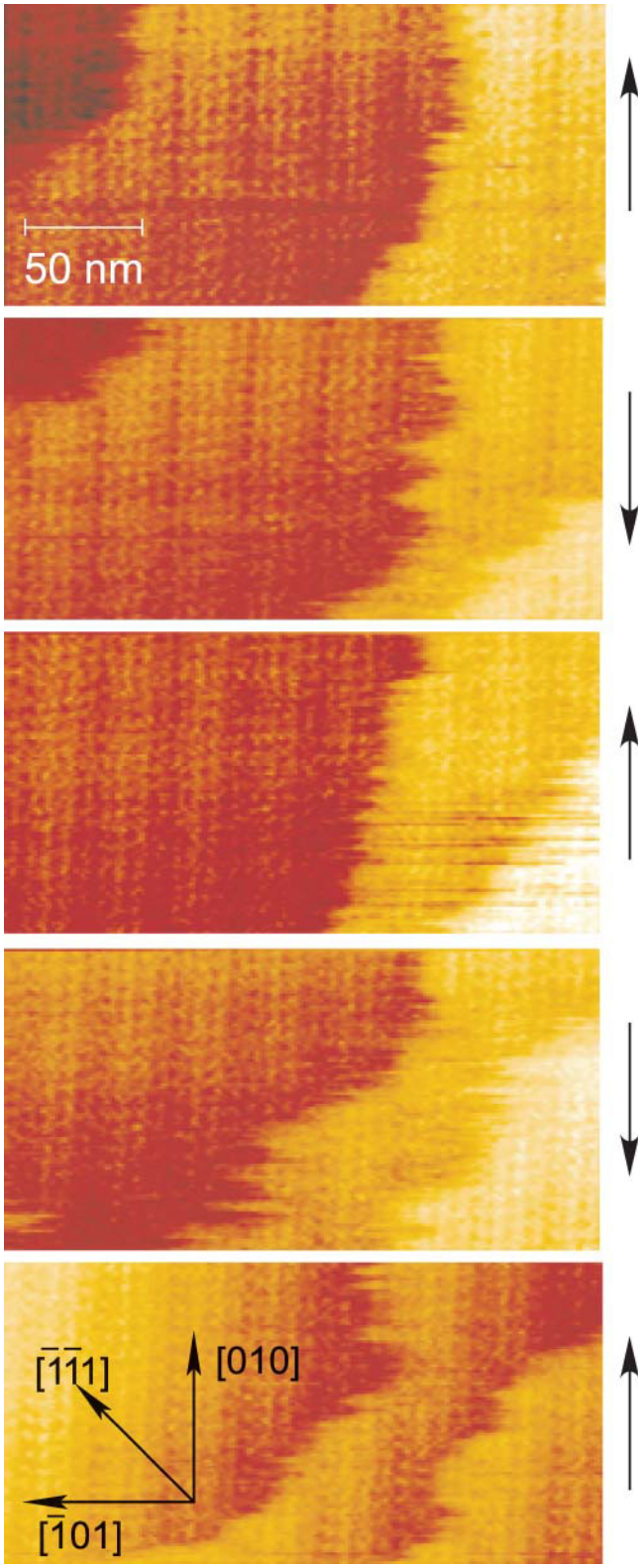

FIGURE 4 A series of molecular resolution images of step propagation. Time between pairs of images is always 35 s. Direction of slow scanning indicated on right side of each panel. Note that the bottom part of the lower step moving in [$\bar{1}$01] direction is significantly faster than step motion in the other directions. $C_{CO\text{-}HbC} = 2.2$ mg mL^{-1}.

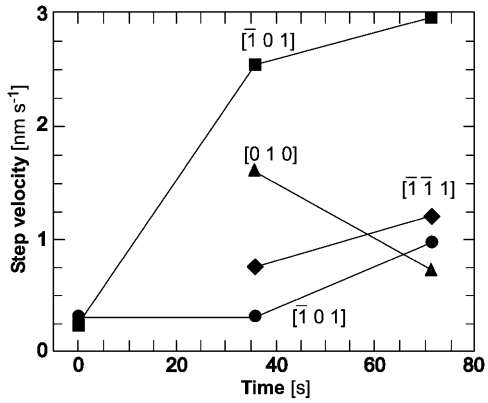

FIGURE 5 Variations of the velocities of the steps in Fig. 4 in three crystallographic directions. Data at 35 s extracted by comparing step locations in the first and third images in Fig. 4; data at 70 s—from step locations in the third and fifth images. Within these pairs, the images were taken with the same scanning direction. The upper data points labeled [$\bar{1}$01] are for the fast lower step in Fig. 4.

$\times 10^{15}$ cm^{-3}, and $\Omega = \frac{1}{4}(54 \times 195 \times 195)$ Å$^3 = 5.1 \times 10^{-19}$ cm^3 (Dewan et al., 2002) is the volume that a molecule occupies in the crystal. We get $\beta \approx 2 \times 10^{-5}$ cm s^{-1}, at the lower end of the range of β for other proteins, $10^{-2} - 10^{-5}$ cm s^{-1} (Reviakine et al., 2003).

Fig. 6 shows that as the steps move along the face, they do not stay equidistant. Areas of high and low step density form. It has been shown that variable step density, also called step bunching, leads to crystal nonuniformity and lower quality and utility of protein crystals (Vekilov and Rosenberger, 1998b).

Impurities and crystal growth

Dynamic light scattering investigations of crystallizing CO-HbC solutions revealed that aggregates of HbC form in solutions of concentrations higher than a few mg mL^{-1}; a typical distribution of the protein species is shown in Fig. 7 *a* (for details about the technique, see Vekilov et al., 2002). In contrast to the distribution in low-concentration HbC solutions, which show a monodisperse sample with a characteristic molecular size of 5.5 nm (Vekilov et al., 2002), the distribution in Fig. 7 *a* shows the presence of at least two populations. The smaller-size population has an apparent mean diameter of 9 nm and these are likely the native HbC molecules. The increase from the typical size of the HbC molecules of 5.5 nm is attributable to the intermolecular attraction in the high-phosphate buffer solution that leads to lower diffusion coefficient (Schmitz, 1990). The lower diffusivity is interpreted by the data-processing algorithms as a size increase (Provencher, 1979, 1982a,b). The larger size population has a mean size of 30 nm and these are likely aggregates of HbC molecules. AFM monitoring of the growth interface revealed that the aggregates are strongly adsorbed at the growth interface,

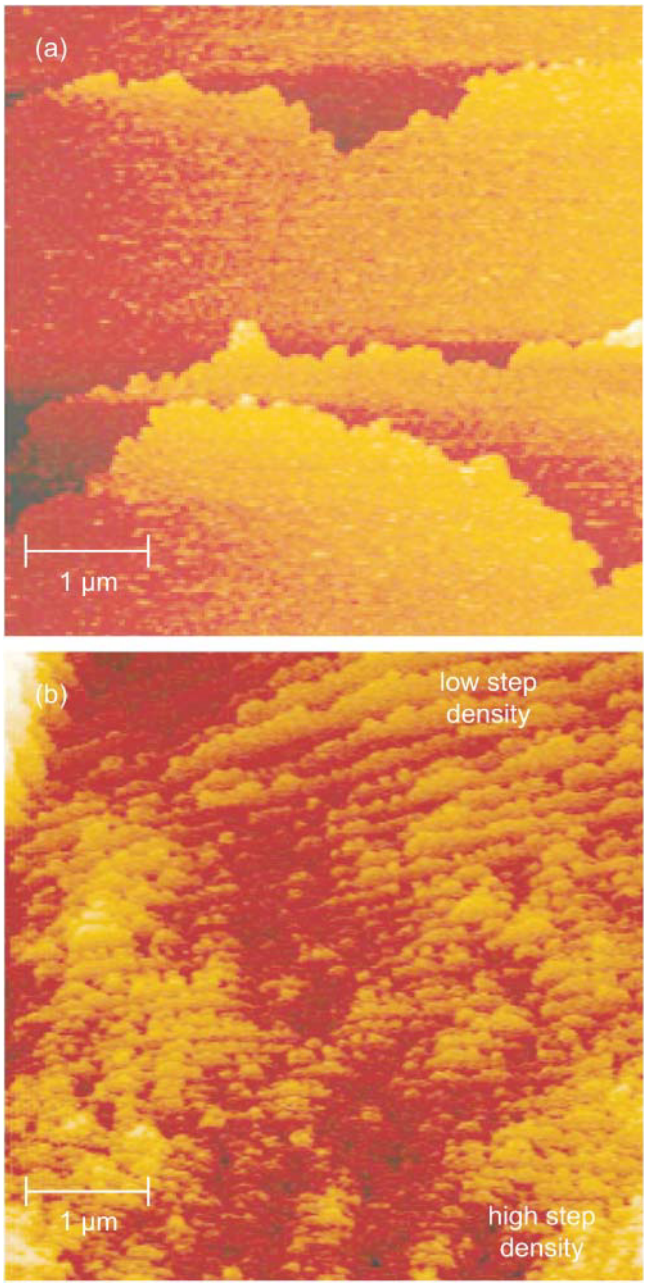

FIGURE 6 Variable density of steps during crystal growth. (*a*) Uniformly low step density at $C_{HbC} = 4$ mg mL^{-1} in 1.9 M phosphate buffer at pH 7.35 at 25°C, i.e., at $C/C_{eq} = 3.3$. (*b*) Regions of high and low step density at $C_{HbC} = 6$ mg mL^{-1}, i.e., at $C/C_{eq} = 5.0$.

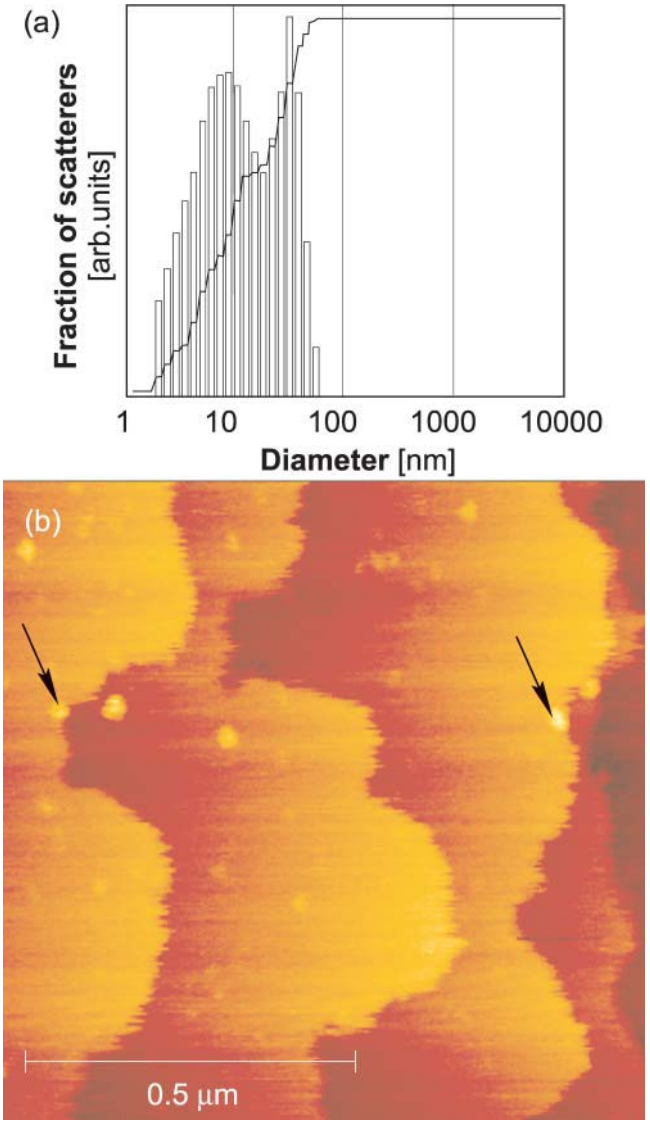

FIGURE 7 HbC aggregates and their effects on growth. (*a*) Dynamic light scattering characterization of a solution of HbC with $C_{CO\text{-}HbC} = 8.5$ mg mL^{-1}. (*b*) Typical image of aggregates of ~30–40 nm adsorbed on the surface at HbC concentration higher than 7–8 mg mL^{-1}. Arrows indicate instances of growth steps pinned by the aggregates.

where they may serve as centers for the nucleation of new crystal layers. Fig. 7 *b* shows that the adsorbed aggregates often pin down the growth layers and slow down their propagation. Cross-section profiles of the images of the aggregates in Fig. 7 *b* and in other images with higher magnification reveal that their vertical dimensions are in the range 10–40 nm (the lateral dimensions may be misleading because of tip-sample convolution effects). This roughly agrees with the 30-nm aggregates detected by the light scattering determination in Fig. 7 *a*.

DISCUSSION

The growth mechanism

The surfaces of crystals, illustrated by Fig. 1 *a*, possess an unexpected feature: four-member strands along the *a* (or *b*) crystallographic axis, separated by well-defined grooves. This arrangement violates the crystallographic symmetry. For better understanding of the suspected reconstruction, in Fig. 1, *b* and *c*, we display the molecular arrangement of the

(101) plane in the crystal bulk. The molecular arrangement of the (101) surface layer compatible with the structure of the crystal bulk in Fig. 1, *b* and *c*, is not unique. If one allows for a surface that contains incomplete crystallographic cells, other arrangements may obtain. For instance, one can add a molecule symmetrically equivalent to the molecule labeled 1 in Fig. 1 *c* in the crevice formed by molecules in positions equivalent to 4, 1, and 2. A second new configuration is produced by adding a molecule in position 2 to the newly formed crevice, and so on. In all cases, the structures reveal four molecules so tightly packed that one of them is partially covered by its neighbor in the $[\bar{1}01]$ direction. None of the produced structures possess the essential feature of Fig. 1 *a*—four-member strands separated by grooves. Thus, we conclude that the surface layer of the crystal, as seen in Fig. 1 *a* and other similar images is ''reconstructed''; numerous instances of reconstruction of the surface layers of inorganic crystals have been documented (Swartzentruber, 1998; Williams and Bartelt, 1991).

The four-molecule-wide strands on the surfaces of the CO-HbC crystals are akin to the two-member strands observed by electron microscopy on the surface of HbS crystals grown from solutions containing PEG (Bluemke et al., 1988; Lessin et al., 1969; Makinen and Sigountos, 1984; Potel et al., 1984). In these studies, the presence of such strands was the main piece of evidence supporting the conclusion of a growth mechanism of HbS crystal involving alignment of the preformed fibers in the solution. Since fibers, ribbons, and other linear objects have been observed in crystallizing solutions of CO-HbC (Hirsch et al., 2001), one may speculate that the observations of the strands support the fiber-alignment mechanism of formation of HbC crystals. However, the results in Figs. 3 and 4 above unambiguously show that the growth of crystals occurs by the attachment of single molecules. In another article (Vekilov et al., 2002), we presented compelling evidence that the nucleation of the CO-HbC crystal is also a process of self-assembly of single molecules and the microribbons and other noncrystalline phases present in the solution only play auxiliary roles in the crystallization process. The overall conclusion emerging from these investigations is that the crystallization mechanisms of HbC, in concentrated phosphate buffer, are by no means different from those found for other proteins (see, e.g., McPherson, 1999; McPherson et al., 2000; Yau et al., 2000a).

Impurities and crystallization

The observations of the impurity effects on the growth of HbC crystals provide some additional insight into a general issue of protein crystallization—that of the nature and role of impurity species. It is commonly thought that crystallization is a method for protein purification. However, there have been numerous crystal growth studies wherein crystal imperfections arise from the incorporation of ''impurities,'' e.g., (Vekilov, 2003). It was found that ''impurities,'' i.e., microheterogeneous molecules of the crystallizing protein, (e.g., aggregates and clusters of this protein, other protein molecules remaining in the solution after isolation and purification, as well as small molecular compounds) affect growth and are often abundantly incorporated into the crystals.

Several detailed studies were carried out with the proteins lysozyme and ferritin (or apoferritin). For both proteins the impurity species that remains in the solution even after laborious purification is a dimer of the native molecules, likely because of its chemical similarity to the native protein (Thomas et al., 1996, 1997, 1998).

With lysozyme, the dimer has an isometric shape and contains two covalently bound monomer chains. It was shown to severely affect the shape of the interface, reduce the growth rate by factors of up to 5, and completely inhibit growth at low supersaturations (Thomas et al., 1996, 1998; Vekilov, 1993; Vekilov et al., 1995; Vekilov and Rosenberger, 1996). It was found that the dimers are preferentially incorporated into the crystals and exhibit severely nonuniform distribution with a core of very high impurity incorporation in the central regions of a crystal (Stojanoff et al., 1997; Vekilov et al., 1996b). It was also found that impurities adsorbed on the growth interface cause severe growth unsteadiness and step bunching (Vekilov and Alexander, 2000; Vekilov et al., 1996a; Vekilov and Rosenberger, 1998a). The nonuniform impurity incorporation and the step bunching have been shown to cause high levels of lattice strain, structural nonuniformities and mosaicity (Caylor et al., 1999; Chernov, 1998, 1999; Dobrianov et al., 1998; Yau et al., 2001).

With ferritin, the ''dimers'' consist of two slightly misfolded native spheres held together by hydrophobic bonds (Petsev et al., 2000). As with lysozyme, they are preferentially incorporated into the crystals (Thomas et al., 2000). Each incorporated dimer causes stacks of trivacancies and single vacancies up to five molecular layers high (Yau et al., 2001, 2000b). The vacancies stress the crystal lattice, and the accumulated strain is resolved by the breaking of crystals larger than 100–200 μm into mosaic blocks of $\sim$50 μm in size (Yau et al., 2001).

The relatively large aggregates of evidence in Fig. 7 are similar to those for crystallization of ferritin and lysozyme in that they consist of the crystallizing protein. In further similarity, the impurities are incorporated into the crystals and severely affect growth. However, there are some significant differences. The HbC aggregates are large and contain multiple native or denatured molecules. While the lysozyme and ferritin dimers exist before crystallization and could, potentially, be removed with a high-sensitivity technique, the HbC aggregates form only after a high-concentration crystallization solution is prepared. Thus, they are a constant companion of crystallization and can only be avoided if a different set of crystallization conditions is employed. While it has been known (Ferre-D-Amare and

Burley, 1994) that protein aggregation should be avoided for successful protein crystallization, it was thought that this is because aggregation provides an alternative pathway to lower the supersaturation of a concentrated protein solution. The above observations with HbC show that even when the aggregate concentration is too low and aggregation cannot be a real competition to crystal formation, aggregates can still interfere with the growth of perfect crystals.

We thank I. Reviakine for help with modeling of the structure of the top crystal layer.

This work is part of the doctoral thesis of Angela R. Feeling-Taylor in partial fulfillment of the requirements for the doctoral degree in the Department of Anatomy and Structural Biology of the Albert Einstein College of Medicine.

This work was supported by the National Heart, Lung, and Blood Institute, National Institutes of Health, through grants HL58038 and HL3865, and National Institutes of Health Minority Predoctoral Fellowship 1F31 HL09564-01 to A.R.F.-T; the Office of Biological and Physical Research, National Aeronautics and Space Administration, through grants NAG8-1354 and NAG8-1854; and the American Heart Association, Heritage Affiliate grant-in-aid No. 9950989T.

REFERENCES

Benedek, G. B., J. Pande, G. M. Thurston, and J. I. Clark. 1999. Theoretical and experimental basis for the inhibition of cataract. *Prog. Retin. Eye Res.* 18:391–402.

Bluemke, D. A., B. Carragher, M. J. Potel, and R. Josephs. 1988. Structural analysis of polymers of sickle cell hemoglobin. II. Sickle hemoglobin macrofibers. *J. Mol. Biol.* 199:333–348.

Bucciantini, M., E. Giannoni, F. Chiti, F. Baroni, L. Formigli, J. Zurdo, N. Taddei, G. Ramponi, C. M. Dobson, and M. Stefani. 2002. Inherent toxicity of aggregates implies a common mechanism for protein misfolding diseases. *Nature.* 416:507–511.

Burton, W. K., N. Cabrera, and F. C. Frank. 1951. The growth of crystals and equilibrium structure of their surfaces. *Philos. Transact. Ser. A. Math. Phys. Eng. Sci* 243:299–360.

Caylor,C. L., I. Dobrianov, S. G. Lemay, C. Kimmer, S. Kriminski, K. D. Finkelstein, W. Zipfler, W. W. Webb, B. R. Thomas, A. A. Chernov and R. E. Thorne. 1999. Macromolecular impurities and disorder in protein crystals. *Proteins.* 36:270–281.

Chandler, D. 2002. Hydrophobicity: two faces of water. *Nature.* 417:491.

Charache, S., C. L. Conley, D. F. Waugh, R. J. Ugoretz, and J. R. Spurrell. 1967. Pathogenesis of hemolytic anemia in homozygous hemoglobin C disease. *J. Clin. Invest.* 46:1795–1811.

Chernov, A. A. 1984. Modern Crystallography III: Crystal Growth. Springer-Verlag, Berlin.

Chernov, A. A. 1998. Crystal growth and crystallography. *Acta. Crystallogr. A.* 54:859–872.

Chernov, A. A. 1999. Estimates of internal stress and related mosaicity in solution grown crystals: proteins. *J. Crystal Growth.* 196:524–534.

Chernov, A. A. 2003. Protein crystals and their growth. *J. Struct. Biol.* 142:3–21.

Dewan J. C., A. Feeling-Taylor, Y. A. Puius, L. Patskovska, Y. Patskovsky, R. L. Nagel, . S. C. Almoa, and R. E. Hirsch.2002. Structure of mutant human carbonmonoxy-hemoglobin C (βE6K) at 2.0 Å resolution. *Acta. Crystallogr. D.* 58:2038–2042.

DeYoreo, J. J., T. A. Land, and B. Dair. 1994. Growth morphology of vicinal hillocks on the {101} face of KH2PO4: from step flow to layer-by-layer growth. *Phys. Rev. Lett.* 73:838–841.

De Yoreo, J. J., T. A. Land, and J. D. Lee. 1997. Limits on surface vicinality and growth rate due to hollow dislocation cores on KDP {101}. *Phys. Rev. Lett.* 78:4462–4465.

Dobrianov, I., K. D. Finkelstein, S. G. Lemay, and R. E. Thorne. 1998. X-ray topographic studies of protein crystal perfection and growth. *Acta Crystallogr. D.* 54:922–937.

Durbin, S. D., and W. E. Carlson. 1992. Lysozyme crystal growth studied by atomic force microscopy. *J. Crystal Growth.* 122:71–79.

Durbin, S. D., and G. Feher. 1996. Protein crystallization. *Annu. Rev. Phys. Chem.* 47:171–204.

Eaton, W. A., and J. Hofrichter. 1990. Sickle cell hemoglobin polimerization. *In* Advances in Protein Chemistry. C. B. Anfinsen, J. T. Edsal, F. M. Richards, and D. S. Eisenberg, editors. Academic Press, San Diego. 63–279.

Eisenberg, D., and W. Kauzmann. 1969. The Structure and Properties of Water. Oxford University Press, New York.

Feeling-Taylor, A. R., R. M. Banish, R. E. Hirsch, and P. G. Vekilov. 1999. Miniaturized scintillation technique for protein solubility determinations. *Rev. Sci. Instrum.* 70:2845–2849.

Ferre-D'Amare, A. R., and S. K. Burley. 1994. Use of dynamic light scattering to assess crystallizability of macromolecules and macromolecular assemblies. *Structure.* 2:357–359.

Giesen, M., G. Schulze Icking-Konert, D. Stapel, and H. Ibach. 1996. Step fluctuations on Pt(111) surfaces. *Surf. Sci.* 366:229–238.

Gratz, A. J., P. E. Hillner, and P. K. Hansma. 1993. Step dynamics and spiral growth on calcite. *Geochim. Cosmochim. Acta.* 57:491–495.

Hirsch, R. E., M. J. Lin, and R. L. Nagel. 1988. The inhibition of hemoglobin C crystallization by hemoglobin F. *J. Biol. Chem.* 263:5936–5939.

Hirsch, R. E., R. E. Samuel, N. A. Fataliev, M. J. Pollack, O. Galkin, P. G. Vekilov, and R. L. Nagel. 2001. Differential pathways in oxy and deoxy HbC aggregation/crystallization. *Proteins.* 42:99–107.

Hunt, J. A., and V. A. Ingram. 1958. Allelomorphism and the chemical differences of the human haemoglobin A, S, and C. *Nature.* 181:1062–1065.

Kelly, J. W. 2000. Mechanisms of amyloidogenesis. *Nat. Struct. Biol.* 7:824–826.

Koo, E. H., P. T. Lansbury, Jr., and J. W. Kelly. 1999. Amyloid diseases: abnormal protein aggregation in neurodegeneration. *Proc. Natl. Acad. Sci. USA.* 96:9989–9990.

Kuznetsov, Y. G., A. J. Malkin, and A. McPherson. 1999. AFM stuides of the nucleation and growth mechanisms of macromolecular crystals. *J. Crystal Growth.* 196:489–502.

Land, T. A., J. J. DeYoreo, and J. D. Lee. 1997. An in-situ AFM investigation of canavalin crystallization kinetics. *Surf. Sci.* 384:136–155.

Lawrence, C., M. E. Fabry, and R. L. Nagel. 1991. The unique red cell heterogeneity of SC disease: crystal formation, dense reticulocytes, and unusual morphology. *Blood.* 78:2104–2112.

Lessin, L. S., W. N. Jensen, and E. Ponder. 1969. Molecular mechanism of hemolytic anemia in homozygous hemoglobin C disease. Electron microscopic study by the freeze-etching technique. *J. Exp. Med.* 130:443–466.

Makinen, M. W., and C. W. Sigountos. 1984. Structural basis and dynamics of the fiber-to-crystal transition of sickle cell hemoglobin. *J. Mol. Biol.* 178:439–476.

Malkin, A. J., Y. G. Kuznetsov, T. A. Land, J. J. DeYoreo, and A. McPherson. 1996. Mechanisms of growth of protein and virus crystals. *Nat. Struct. Biol.* 2:956–959.

McPherson, A. 1999. Crystallization of biological macromolecules. Cold Spring Harbor Laboratory Press, Cold Spring Harbor, New York.

McPherson, A., A. J. Malkin, and Y. G. Kuznetsov. 2000. Atomic force microscopy in the study of macromolecular crystal growth. *Annu. Rev. Biophys. Biomol. Struct.* 29:361–410.

Nagel, R. L., and C. Lawrence. 1991. The distinct pathobiology of SC disease: therapeutic implications. *In* Hematology/Oncology Clinics of North America. R. L. Nagel, editor. W. B. Saunders, Philadelphia.

Petsev, D. N., B. R. Thomas, S.-T. Yau, and P. G. Vekilov. 2000. Interactions and aggregation of apoferritin molecules in solution: effects of added electrolytes. *Biophys. J.* 78:2060–2069.

Potel, M. J., T. E. Wellems, R. J. Vassar, B. Deer, and R. Josephs. 1984. Macrofiber structure and the dynamics of sickle cell hemoglobin crystallization. *J. Mol. Biol.* 177:819–839.

Provencher, S. W. 1979. Inverse problems in polymer characterization; direct analysis of polydispersity with photon correlation spectroscopy. *Makromol. Chem.* 180:201–209.

Provencher, S. W. 1982a. A constrained regularization method for inverting data represented by linear algebraic equations. *Comput. Phys. Commun.* 27:213–227.

Provencher, S. W. 1982b. CONTIN: a general purpose constrained regularization program for inverting noisy linear algebraic and integral equations. *Comput. Phys. Commun.* 27:229–242.

Reviakine, I., D. K. Georgiou, and P. G. Vekilov. 2003. Capillarity effects on the crystallization kinetics: insulin. *J. Am. Chem. Soc.* 125:11684–11693.

Schmitz, K. S. 1990. Dynamic Light Scattering by Macromolecules. Academic Press, New York.

Stojanoff, V., D. P. Siddons, L. A. Monaco, P. G. Vekilov, and F. Rosenberger. 1997. X-ray topography of tetragonal lysozyme grown by the temperature controlled technique. *Acta Crystallogr. D.* 53:588–595.

Swartzentruber, B. S. 1998. Fundamentals of surface step and island formation mechanisms. *J. Crystal Growth.* 188:1–10.

Teng, H. H., P. M. Dove, C. A. Orme, and J. J. De Yoreo. 1998. Thermodynamics of calcite growth: baseline for understanding biomineral formation. *Science.* 282:724–727.

Thomas, B. R., D. Carter, and F. Rosenberger. 1997. Effects of microheterogeneity on horse spleen apoferritin crystallization. *J. Crystal Growth.* 187:499–510.

Thomas, B. R., A. A. Chernov, P. G. Vekilov, and D. C. Carter. 2000. Distribution coefficients of protein impurities in ferritin and lysozyme crystals. Self-purification in microgravity. *J. Crystal Growth.* 211:149–156.

Thomas, B. R., P. G. Vekilov, and F. Rosenberger. 1996. Heterogeneity determination and purification of commercial hen egg white lysozyme. *Acta. Crystallogr. D.* 52:776–784.

Thomas, B. R., P. G. Vekilov, and F. Rosenberger. 1998. Effects of microheterogeneity on hen egg white lysozyme crystallization. *Acta. Crystallogr. D.* 54:226–236.

Van den Hoek, B., J. P. Van der Eerden, and P. Bennema. 1982. Thermodynamic stability conditions for the occurrence of hollow cores caused by stress of line and planar defects. *J. Crystal Growth.* 56:621–632.

Vekilov, P. G. 1993. Elementary processes of protein crystal growth. *In* Studies and Concepts in Crystal Growth. H. Komatsu, editor. Pergamon Press, Oxford, UK. 25–49.

Vekilov, P. G. 2003. Solvent entropy effects in the formation of protein solid phases. *In* Methods in Enzymology. R. M. Sweet, editor. Academic Press, San Diego. 84–105.

Vekilov, P. G., and J. I. D. Alexander. 2000. Dynamics of layer growth in protein crystallization. *Chem. Rev.* 100:2061–2089.

Vekilov, P. G., J. I. D. Alexander, and F. Rosenberger. 1996a. Nonlinear response of layer growth dynamics in the mixed kinetics-bulk transport regime. *Phys. Rev. E.* 54:6650–6660.

Vekilov, P. G., and A. A. Chernov. 2002. The physics of protein crystallization. *In* Solid State Physics. H. Ehrenreich, F. Spaepen, editors. Academic Press, New York. 1–147.

Vekilov, P. G., A. Feeling-Taylor, and R. E. Hirsch. 2003. Nucleation and growth of crystals of hemoglobins: case of HbC. *In* Methods in Hemoglobin Disorders. Series in Molecular Medicine. R. L. Nagel, editor. Humana Press, Totowa, NJ.

Vekilov, P. G., A. R. Feeling-Taylor, D. N. Petsev, O. Galkin, R. L. Nagel, and R. E. Hirsch. 2002. Intermolecular interactions, nucleation and thermodynamics of crystallization of hemoglobin C. *Biophys. J.* 83: 1147–1156.

Vekilov, P. G., Y. G. Kuznetsov, and A. A. Chernov. 1990. Dissolution morphology and kinetics of (101) ADP face; mild etching of surface defects. *J. Crystal Growth.* 102:706–716.

Vekilov, P. G., L. A. Monaco, and F. Rosenberger. 1995. Facet morphology response to non-uniformities in nutrient and impurity supply. I. Experiments and interpretation. *J. Crystal Growth.* 156:267–278.

Vekilov, P. G., L. A. Monaco, B. R. Thomas, V. Stojanoff, and F. Rosenberger. 1996b. Repartitioning of NaCl and protein impurities in lysozyme crystallization. *Acta Crystallogr. D.* 52:785–798.

Vekilov, P. G., and F. Rosenberger. 1996. Dependence of lysozyme growth kinetics on step sources and impurities. *J. Crystal Growth.* 158:540–551.

Vekilov, P. G., and F. Rosenberger. 1998a. Increased stability in crystal growth kinetics in response to bulk transport enhancement. *Phys. Rev. Lett.* 80:2654–2656.

Vekilov, P. G., and F. Rosenberger. 1998b. Intrinsic kinetics fluctuations as cause of growth inhomogeneity in protein crystals. *Phys. Rev. E.* 57:6979–6981.

Volmer, M. 1939. Kinetik der Phasenbildung. Steinkopff, Dresden.

Williams, E. D., and N. C. Bartelt. 1991. Thermodynamics of surface morphology. *Science.* 251:393–400.

Yau, S.-T., D. N. Petsev, B. R. Thomas, and P. G. Vekilov. 2000a. Molecular-level thermodynamic and kinetic parameters for the self-assembly of apoferritin molecules into crystals. *J. Mol. Biol.* 303:667–678.

Yau, S.-T., B. R. Thomas, O. Galkin, O. Gliko, and P. G. Vekilov. 2001. Molecular mechanisms of microheterogeneity-induced defect formation in ferritin crystallization. *Proteins.* 43:343–352.

Yau, S.-T., B. R. Thomas, and P. G. Vekilov. 2000b. Molecular mechanisms of crystallization and defect formation. *Phys. Rev. Lett.* 85:353–356.

Yip, C. M., and M. D. Ward. 1996. Atomic force microscopy of insulin single crystals: direct visualization of molecules and crystal growth. *Biophys. J.* 71:1071–1078.